

Near-Infrared Photometry in J H and Kn bands for Polar Ring Galaxies:

II. Global Properties

Enrichetta Iodice,^{1,2}, Magda Arnaboldi¹, Linda S. Sparke³, and Kenneth C. Freeman⁴

¹ INAF-Osservatorio Astronomico di Capodimonte (OAC), via Moiariello 16, I-80131 Napoli

² International School for Advanced Studied (ISAS), via Beirut 2-4, I-34014 Trieste

³ University of Wisconsin, Department of Astronomy, 475 N. Charter St., Madison, WI

⁴ RSAA, Mt. Stromlo Observatory, Canberra, Cotter Road,
Weston ACT 2611, Australia

Received ; accepted

Abstract. We discuss the properties of the host galaxy and ring light distributions in the optical and near infrared bands for a sample of Polar Ring Galaxies (PRGs), presented in Paper I (Iodice et al. 2002b). The goal of this work is to test different formation scenarios for PRGs, proposed by different authors in the last decades, by comparing their predictions with these new data. The strategy is twofold: *i*) the integrated colors of the main components in these systems are compared with those of standard morphological galaxy types, to investigate whether differences in colors are caused by dust absorption or difference in stellar populations. We then derived an estimate of the stellar population ages in PRGs, which can be used to set constrains on the dynamical modeling and the time evolution of these systems; *ii*) we analyse the structural parameters of the host galaxy in order to understand whether this component is a standard early-type system as its morphology suggests, and the light distribution in the polar ring to measure its radial extension.

These observational results indicate that the global properties of PRGs are better explained by dissipative merging of disks with un-equal masses as proposed by Bekki (1998), rather than the accretion-or stripping-of gas by a pre-existing early-type galaxy.

Key words. Galaxies: peculiar – Galaxies: photometry – Galaxies: evolution – Galaxies: formation

1. Introduction

Gravitational interactions and mergers affect the morphologies and dynamics of galaxies. Both the Hubble Space Telescope (HST) and the ESO Very Large Telescope (VLT) make it possible to observe the early universe and show that these processes dominate at higher redshift (Driver et al. 1995). Polar Ring Galaxies (PRGs) are considered one of the best example of remnants from galaxy interaction. These peculiar objects are composed by a central spheroidal component, the *host galaxy*, surrounded by an outer *ring*, made up by gas, stars and dust, in a nearly perpendicular plane to the equatorial one of the central galaxy (Whitmore et al. 1990). The origin of PRGs is still an open debate: they may be the result of an accretion phenomena (Toomre 1977; Shane 1980; Schweizer et al. 1983; Sackett 1991; Sparke 1991; Hibbard & Mihos 1995;

Reshetnikov and Sotnikova 1997) or of major dissipative merger (Bekki 1997; 1998). Recent observations of several interacting galaxy pairs, of similar luminosities, display ring-like structures (e.g. NGC 7464/65, Li & Seaquist 1994; NGC 3808A,B and NGC 6285/86, Reshetnikov et al. 1996).

Reshetnikov & Sotnikova (1997) studied the accretion scenario for the formation of PRGs using a smoothed-particle hydrodynamic simulations (SPH) in high speed encounters. They analyzed the different ring morphologies which were generated by the encounter of a gas-rich spiral with either an elliptical or an S0 galaxy. They followed the full history of the gas stripping: from the spiral galaxy outskirts to its capture by the early-type galaxy, on a parabolic encounter. The total amount of accreted gas by the early-type object is about 10% of the gas in the spiral galaxy, i.e. up to $10^9 M_{\odot}$. The size of the polar ring is found to be related to the central mass (luminous + dark) concentration of the host galaxy. If the mass is

highly concentrated, i.e. the elliptical galaxy case, the ring forms at smaller radii; if the host galaxy has an extended massive halo, i.e. the S0 case, the ring average radius (\bar{R}) can be as large as 30 kpc. This scenario can account for the formation of (quasi-)stable polar rings, whose radial extent is of the order of 10% of the ring extent.

A quite different approach to the formation of polar ring galaxies was recently proposed by Bekki (1998). In this scenario, the polar ring results from a “polar” merger of two disk galaxies with unequal mass. The “intruder”, on a polar orbit with respect to the “victim” disk, passes through it near its center: it is slowed down, and pulled back toward the victim, by strong dissipation which is caused by the interaction with the victim gaseous disk. Dissipation removes random kinetic energy from the gaseous component of the victim’s disk, so that some gas can settle again into a disk configuration. The morphology of the merger remnants depends on the merging initial orbital parameters and the initial mass ratio of the two galaxies.

Bekki’s scenario successfully reproduces the range of observed morphologies for polar ring galaxies, such as the existence of both wide and narrow rings, helical rings and double rings (Whitmore 1991). Furthermore, this scenario would also explain the presence of wide and massive polar disk, as observed in NGC 4650A (Arnaboldi et al. 1997, Iodice et al. 2002a; Gallagher et al. 2002). The two scenarios, accretion vs. dissipative mergers of disks, both predict the general features of PRGs: a structure-less appearance of the host galaxy, and the younger dustier appearance of the polar structure. But they differ on their predictions about structural parameters, age, baryonic mass and polar structure extension. Therefore, the two scenarios should be tested against the observed properties of both wide and narrow PRGs, in particular their observed structural parameters, colors and total light. Given that PRGs contain a lot of dust, we must study their light distribution in the near-infrared (NIR), and determine the distribution of their evolved stellar population. To this aim, new NIR data for a sample of PRGs were collected and analysed in Iodice et al. 2002b, hereafter Paper I. In this work we compare the integrated colors derived for the host galaxy and ring of each PRG in our sample (see Sec.5 in Paper I) with those of standard morphological galaxy types, in Sec.2, and compute an estimate of the stellar population ages, in Sec.3. In Sec. 4 and Sec. 5, we perform a detailed analysis of the light distribution properties in the host galaxy and ring. The new observational evidences obtained for this sample of PRGs are summarized in Sec. 6, and conclusions are derived in Sec. 7.

2. NIR colors

The near-infrared J, H and Kn images for a sample of PRGs were obtained at the 2.3 m telescope of the Mt. Stromlo and Siding Spring Observatory, with the CASPIR camera; all PRGs in our sample are listed in Table 1. A detailed description of the observations and data reduction

were given in Paper I (see Sec. 2). For each object, we computed the integrated magnitudes in J, H and Kn bands, in five different areas (shown in Fig. 8, Paper I), which cover the nucleus of the system, the host galaxy stellar component (outside the nucleus), and the polar structure (see Paper I, Sec.5 for more details).

We then derived the J-H vs. H-K integrated colors for the host galaxy and ring, see Paper I, Sec. 5. We now compare them with those of (1) standard early-type galaxies in the Fornax and Virgo clusters (Persson et al., 1979), (2) spirals (Giovanardi & Hunt, 1996; Frogel, 1985; de Jong & van der Kruit, 1994), (3) dwarf ellipticals (Thuan, 1985), (4) low surface brightness galaxies, LSB, (Bergvall et al. 1999), and with the inner regions of Seyfert 1 and 2 (Glass and Moorwood, 1985), see Fig.1. In all PRGs of our sample, the host galaxy has on average bluer colors than the typical values for early-type galaxies. They are more similar to the colors of spiral and dwarf galaxies, with the exception of AM 2020-504. This component is also characterized by a strong color gradient toward bluer colors in J-H, from the central regions going outwards. The outer regions have on average similar H-K colors.

In the screen model approximation, we can compute the reddening vector by assuming $A_V = 0.3$, as in the Milky Way galaxy (Gordon, Calzetti & Witt 1997); the result is shown in Fig.1. It suggests that the dust reddening is small in these bands, and it can account for the observed color gradient between nucleus and stellar component in the host galaxy, with the exception of ESO 603-G21, and within the uncertainties of the color estimate. The central regions of ESO 603-G21 have colors which are typical of a Seyfert galaxy, as it was found by Arnaboldi et al. in 1995. Similar behavior is observed for the nuclear region of ESO 415-G26.

In almost all PRGs, the polar structure has on average bluer colors than the host galaxy, and quite similar to those of the late-type galaxies.

We then have derived the B-H vs. J-K integrated colors for the host galaxy and ring, which are shown in Fig.2. The host galaxy in all PRGs of the sample, but AM 2020-504, has overall bluer B-H colors than the average values observed in early-type galaxies (Bothun & Gregg 1990); on average, they are very similar to those of spirals (by Bothun et al., 1984). We can then expect a younger age for the central component of PRGs than those predicted for early-type systems. In nearly all objects, one side of the host galaxy is bluer than the other side: this is most likely caused by the presence of the polar ring, which perturbs the regions where it passes in front of the galaxy, along the line-of-sight.

As was already found in the J-H vs H-K diagram, there is a strong color gradient between the central region of the host galaxy and its outer parts, for all PRGs of the sample. The very red B-H colors of nuclear regions may be due to the dust absorption: as extreme examples, in the central regions of ARP 230 most of light is completely obscured by dust in the optical band. The reddening vector, shown on Fig.2, is also computed for these color indices:

Table 1. PRG sample.

Object	α (J2000)	δ (J2000)	Filter
A0136-0801	01h38m55.2s	-07d45m56s	H
ESO 415-G26	02h28m20.1s	-31d52m51s	JHK _n
ARP 230	00h46m24.2s	-13d26m32s	JHK _n
AM 2020-504	20h23m54.8s	-50d39m05s	JHK _n
ESO 603-G21	22h51m22.0s	-20d14m51s	JHK _n

the absorption due to the dust may account for the color gradient in the host galaxy of almost all PRGs.

3. Using colors to date the stellar populations in PRGs

The next step is to compare the B-H vs. J-K integrated colors with the stellar population models. The goal is to derive the ages of the dominant stellar populations in the central spheroid and polar structure. The B-H and J-K colors are used to break the age-metallicity degeneracy, as suggested by Bothun et al. (1984). The J-K color gives a good estimate of the metallicity and it is quite insensitive to the presence of a young stellar population. This effect is also supported by the observed monotonic increase of the mean J-K color in globular clusters with increasing metallicity (Aaronson et al. 1978, Frogel et al. 1983). In addition, the population synthesis models by Bothun (1982) show that J-K is decreased only by 0.05 mag as a result of a star burst, while the B luminosity is increased by 1 mag by the same stellar burst. The B-H color is sensitive to the combined effect of the Star Formation Rate (SFR), metallicity and age (Bothun et al. 1984).

The stellar population synthesis model developed by Bruzual & Charlot (1993), GISSEL (*Galaxies Isochrone Synthesis Spectral Evolution Library*) was used to reproduce the integrated colors of different regions (see Sec.2) in each PRGs of the sample. We first select a set of models which were able to reproduce on average the integrated colors of galaxies with different morphological types in the local Universe. These models were then optimized to reproduce the observed colors for the main components of each PRG. The GISSEL key input parameters are the Initial Mass Function (IMF), the Star Formation Rate (SFR), and the metallicity. In what follows, we have assumed that stars form according to the Salpeter (1955) IMF, in the range from 0.1 to $125M_{\odot}$.

To derive the age estimate for the polar structure and host galaxy, different evolutionary models are adopted, given by different SFRs. A star formation history with an exponentially decreasing rate, given by $SFR(t) = \frac{1}{\tau} \exp(-t/\tau)$, was adopted for the central host galaxy. The τ parameter quantifies the “time scale” when the star formation was most efficient. The adopted expression for the SFR is used to reproduce the photometric properties of the elliptical galaxies, and can be derived from the assumption that the rate with which stars form is proportional to the available gas quantity (Kennicutt, 1983). In order to obtain the largest range for the age estimate,

the following two values were adopted for the time scale parameter: $\tau = 1$ Gyr and $\tau = 7$ Gyr. Each model for the host galaxy were derived for the following metallicity values: $Z = 0.0004$, $Z = 0.008$, $Z = 0.02$, $Z = 0.05$, $Z = 0.1$, which are constant with age. The corresponding evolutionary tracks were derived for each metallicity and are plotted in Fig. 2 with the lines of constant age.

The photometric properties of a sample of early-type galaxies by Bothun et al. (1984) are well reproduced with a $\tau = 1$ Gyr model, which predicts an age of about 10 Gyr for the dominant stellar population in these systems. On the other hand, the same model predicts younger ages, between 1 to 3 Gyr, for the host galaxy (nucleus and outer stellar component) in all PRGs of this sample. The exception is AM 2020-504, which seems to be as old as standard early-type galaxies, see Fig. 2. For the sample of early-type galaxies and the polar ring galaxy AM 2020-504, the model with $\tau = 7$ Gyr implies an age older than 10 Gyr, whereas the other PRGs of the sample have younger age, between 1 to 3 Gyr, see Fig. 2.

On average, the polar structure has bluer colors than the host galaxy, which suggests even a younger age for this component. Observations of HII regions and blue star clusters associated with the polar component suggest that star formation is active in polar rings, so a constant star formation rate, $SFR(t) = K$ with $K \sim 10^{-10} M_{\odot}/yr$, (with metallicities $Z = 0.0004$, $Z = 0.008$, $Z = 0.02$, $Z = 0.05$, $Z = 0.1$) was adopted. For each metallicity, the corresponding evolutionary tracks were obtained and the lines of constant age derived, see Fig. 3. These models successfully reproduce the mean colors for a sample of spiral galaxies (Bothun et al., 1984) and imply an average age of about 5 Gyr for these objects. The integrated colors of the polar structure in all PRGs of this sample are very similar to the bluer/younger spiral galaxies; they are also clustered in the same metallicity range, between $Z = 0.02$ and $Z = 0.05$, and similar age of about 1 Gyr.

We wish to stress that the colors derived for both components were not corrected for the intrinsic reddening due to the PR system, i.e. the absorption caused by the dust in the polar structure; therefore the true colors of the stellar population associated with the central host galaxy might be even bluer. Furthermore, the age estimates for the host galaxy and the polar structure are uncertain, because we do not have independent information on the star formation law and metallicity of the stellar population in the two components. The intrinsic uncertainties of the synthesis population models must also be considered, particularly for the age of the host galaxy. By comparing three recent synthesis codes, Charlot, Worthey and Bressan (1996) found that the colors predicted for old populations with an age > 1 Gyr, with the same input age and metallicity, are affected by discrepancies, which are primarily due to the different prescriptions adopted for the stellar evolution theory. Thus, the age estimates given here, for the central host galaxy and polar structure, should be considered only indicative.

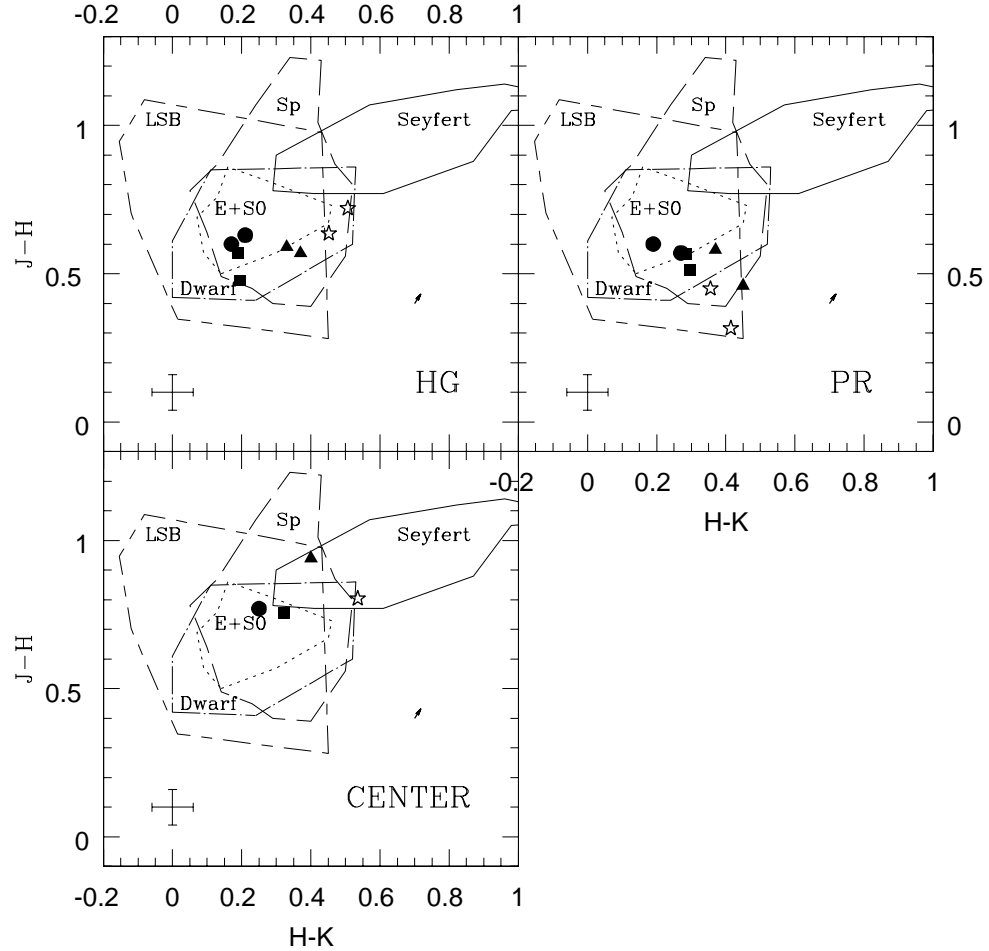


Fig. 1. J-H vs. H-K color diagram for the two regions of the host galaxy (top left panel), two regions for the polar ring (top right panel) and for the central area (bottom left panel) in all PRGs of our sample. Code for symbols is: stars for ESO 415-G26, filled squares for ARP 230, filled circles for AM 2020-504 and filled triangles for ESO 603-G21. The dotted contour limits the region where the integrated colors of Es and S0s are found; the long-dashed contour limits the region where the integrated colors of spirals are found; the dashed-dotted contour identifies the integrated colors of the dwarf elliptical galaxies; the long dashed - short dashed contour identifies the integrated colors of LSB galaxies, and the continuous line limits the integrated colors of the nuclear regions of Seyfert 1 and 2 galaxies. The arrow, in the lower right corner, indicates the reddening vector direction computed for galactic dust in the screen model approximation, see discussion in Sec.2. The average errors are shown in the lower left corner.

4. Study of the host galaxy light distribution

One of the open issues in the study of PRGs is the nature of the host galaxy. A qualitative morphological inspection suggests that this component is similar to an early-type galaxy, most often an S0 (see Paper I, Sec. 3). However, the NIR integrated colors, derived for the host galaxy in this work (Sec.2) and in previous ones (Arnaboldi et al. 1995, Iodice et al. 2002a), are bluer on average than those for standard early-type galaxies. The study of the surface brightness light distribution in the host galaxy may

represent an independent way to check whether this component is really an S0 galaxy or not, by investigating how the structural parameters compare with those of standard early-type galaxies.

4.1. Bulge effective parameters: μ_e - $\log r_e$ plane

In Fig. 4 (left panel) we plot the structural parameters of PRG host galaxies in the μ_e and $\log r_e$ plane. We select a sample of S0 and spiral galaxies for the comparison. The sample of early-type galaxies were studied by Bothun and

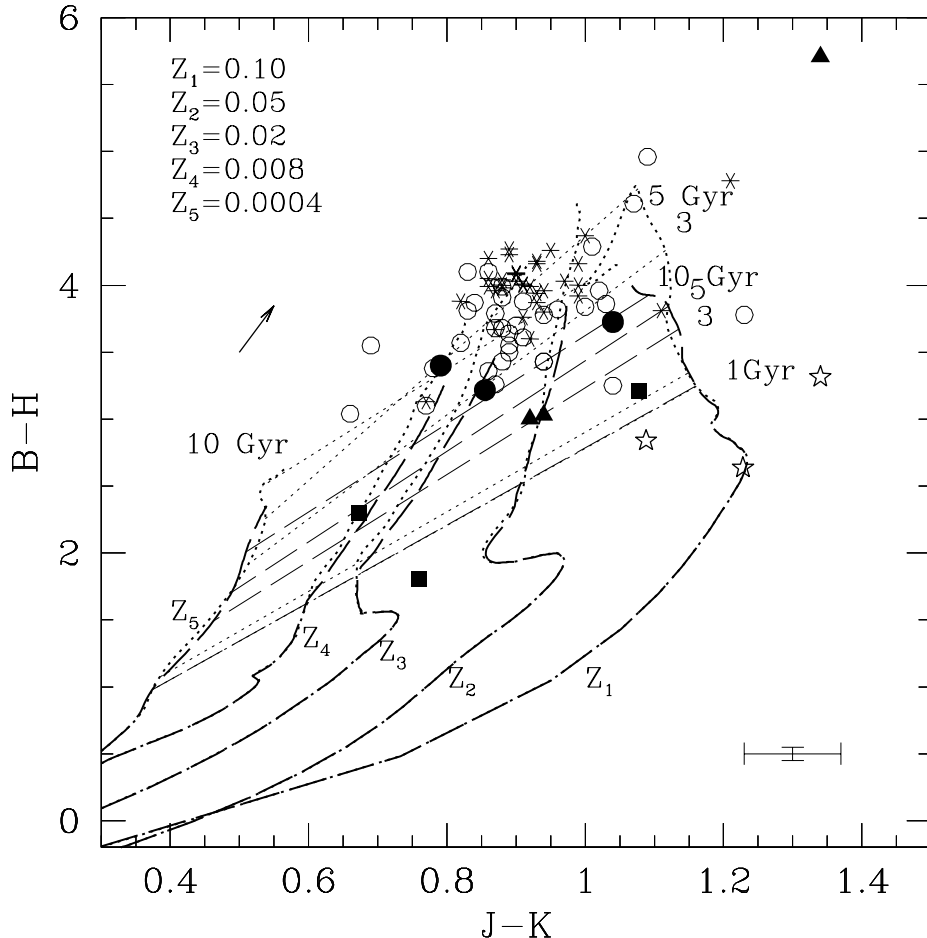


Fig. 2. B-H vs. J-K color diagram of the evolutionary tracks for the stellar synthesis models optimized for the host galaxy, for each PRG of the sample. Code for symbols is the same adopted in Fig.1. The arrow (on the left side) indicates the reddening vector direction for galactic dust and the screen model approximation, quoted in Sec.5 of Paper I. The average errors are indicated in the bottom right side. The heavier dotted lines correspond to models with a characteristic timescale $\tau = 1\text{Gyr}$ and heavier dashed lines for models with $\tau = 7\text{Gyr}$. Models are computed for different metallicities as shown on this figure. Light dotted and light dashed lines indicate loci of constant age for the different models; different ages are reported on the plot. Open circles and asterisks correspond to bulges and disks respectively from a sample of S0 galaxies (Bothun & Gregg 1990).

Gregg (in 1990). The structural parameters for these objects were obtained by fitting the light distribution with the super-position of a de Vaucouleurs law ($n = 4$) and an exponential disk, for the bulge and disk component respectively, in the B band. The surface brightness parameters in the K band are derived by considering the average B-K color of these objects (Bothun and Gregg, 1990). The sample of spiral galaxies include objects studied by Möllenhoff & Heidt (2001) and by Khosroshahi et al. (2000). The host galaxy of PRGs are characterized by a more “compact” bulge with respect to normal early-type galaxies, except for AM 2020-504 which has larger values

of μ_e and r_e . Reshetnikov et al. (1994) found a similar behavior for the bulges of polar ring galaxies in the B band. Because PRGs have smaller bulges also in the NIR, where the perturbations due to the dust absorption are minimal, we know now that the PRG bulges are indeed smaller¹. The 2D bulge-disk decomposition adopted here (see Sec.6, Paper I) allow us to minimize the perturbations due to the ring and to conclude that the bulge component of the host

¹ Reshetnikov et al. (1994) were not able to exclude the hypothesis that the bulge luminosities and sizes were underestimated because of dust absorption by the polar ring.

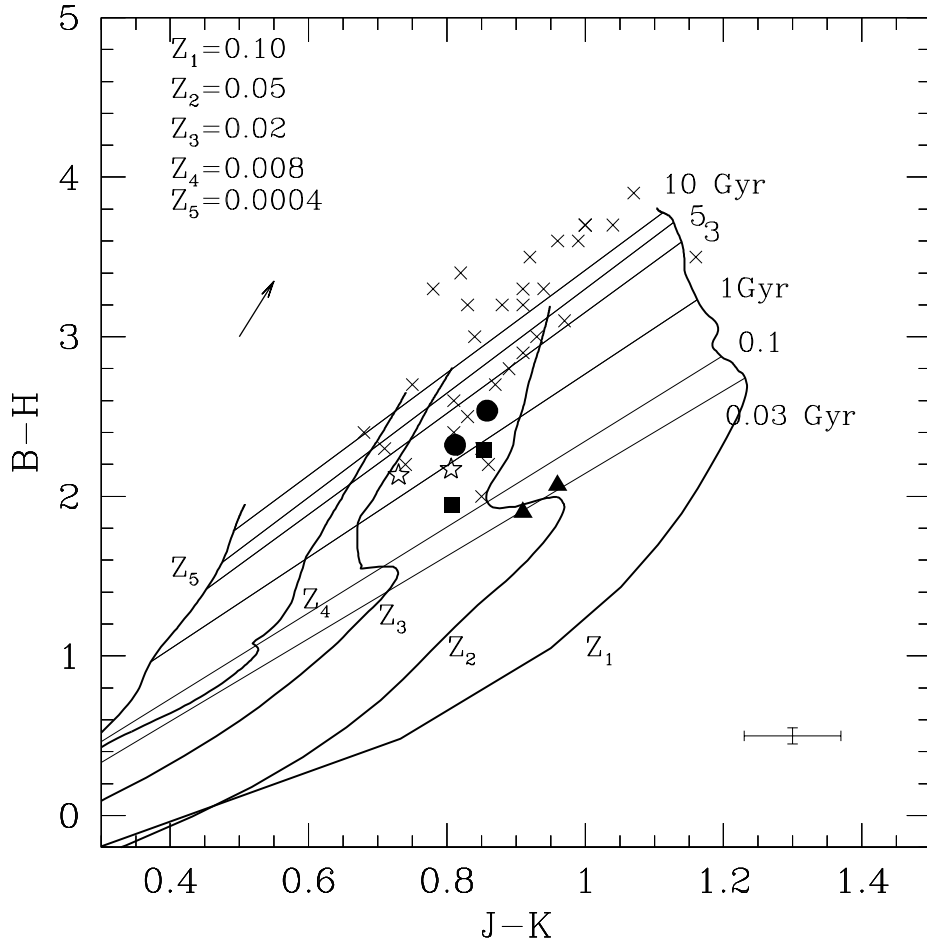


Fig. 3. B-H vs. J-K color diagram of the evolutionary tracks for the stellar synthesis models optimized for the polar structure, for each PRG of the sample. Code for symbols is the same adopted in Fig.1. The arrow (on the left side) indicates the reddening vector direction for galactic dust and the screen model approximation, quoted in Sec.5 of Paper I. The average errors are indicated in the bottom right side. Heavier lines indicate models with constant SFR, computed for different metallicities (reported on the plot). Light lines are loci of constant age; different ages are quoted on the plot. Crosses are for a sample of spiral galaxies (Bothun et al., 1984).

galaxy in PRGs resembles the smallest early-type galaxies with the higher surface brightness in the μ_e - $\log r_e$ plane.

4.2. Bulge scale parameters: $\log n$ - $\log r_e$ plane

The optical light distribution in the bulge of the host galaxy has a quasi-exponential behavior, as suggested by the small values of the n exponent (close to 1), in all PRGs of the sample, except for AM 2020-504 (see also Table 6, Paper I). In Fig. 4 (right panel) we show the comparison between the scale parameters n and r_e for the bulge component in PRGs, with those for a sample of early-type galaxies in the Virgo cluster (Caon et al., 1993), for spiral galaxies (Möllenhoff & Heidt 2001; Khosroshahi et al.

2000) and for a sample of early type galaxies of low surface brightness (Davies et al. 1988) in the Fornax cluster. Since Davies et al. (1988) fit the B band light profiles by adopting the generalized de Vaucouleurs law in the form $I(r) = I_0 \exp[-(r/A)^N]$, we have computed the effective radius r_e and the exponent n from this scalelength radius A and the exponent N .

In this plane, PRGs fall in the region where lower values for both parameters are found, together with the LBS and spiral galaxies. The PRGs bulge scale parameters seem to “follow” the relation between the n exponent and the effective radius, found by Caon et al. (1993), for which n increases steadily with r_e . The polar ring galaxy AM 2020-504 is the only object of the sample which falls in

the same regions occupied by “ordinary family” of early-type galaxies (Capaccioli et al. (1992)).

In their NIR study of spiral galaxies Möllenhoff & Heidt (2001) have shown that the n exponent and effective radius correlates with the Hubble types, and that late-type spirals are characterized by the lowest values of the n exponent and have the smaller bulges. The PRG bulge scale parameters correspond to those of the late-type galaxies. However, the shape parameter n derived for PRGs must be considered as a lower limit: we have found that the light in PRGs bulges is very concentrated toward the center, so the convolution of such light distribution with the PSF may cause a smoothing of the light profiles toward the center, leading to a biased small value for the n exponent.

4.3. Photometric plane for bulges

Khosroshahi et al. (2000) found that a single photometric plane exists in the space of structural parameters describing both Ellipticals and bulges of early-type spiral galaxies. They showed that $\log n$, $\log r_{eff}$ and the central surface brightness $\mu_b(0)$ are related by the equation $\log n = (0.172 \pm 0.020) \log r_{eff} - (0.069 \pm 0.004) \mu_b(0) + (1.18 \pm 0.04)$, which is the best-fit plane for elliptical galaxies and the bulges of spiral galaxies. The photometric plane was used to constrain the bulge formation mechanisms in galaxies. Möllenhoff & Heidt (2001) found that late-type disk galaxies also share this single plane, and they stressed that this is a further hint to a common mechanism for bulge formation in all type of galaxies.

In the left panel of Fig. 5 we plot the photometric plane for bulges of spiral galaxies (by Khosroshahi et al. 2000 and Möllenhoff & Heidt 2001) for the host galaxy in PRGs of our sample. AM 2020-504 is the only PRG which shares the same plane of spiral and elliptical galaxies galaxies. The other PRGs of the sample fall away from this plane, in the lower-left corner, which is not as widely populated by the standard type of galaxies.

4.4. Disk structural parameters: μ_0 - $\log r_h$ plane

The average value of the central surface brightness (corrected for the inclination, see Sec.6, Paper I) for this sample of PRGs is $\langle \mu_0^c \rangle = 15.9 \pm 0.3$ mag arcsec $^{-2}$. This value is brighter than the average value for the S0 galaxies (by Bothun and Gregg² 1990), which is $\langle \mu_0^c \rangle = 16.6 \pm 0.9$ mag arcsec $^{-2}$, and for spiral galaxies (by Möllenhoff & Heidt 2001), which is $\langle \mu_0^c \rangle = 18 \pm 1$ mag arcsec $^{-2}$. The average scalelength of the disks in the host galaxy is $\langle r_h \rangle = 1.0 \pm 0.6$ kpc, whereas the average value for this sample of S0 galaxies is $\langle r_h \rangle = 3 \pm 1$ kpc and for spiral galaxies is $\langle r_h \rangle = 4.5 \pm 2$ kpc. Disks in the PRG host galaxy are brighter and smaller than the disks of S0 galaxies: this is clearly evident in Fig. 5 (right panel), which

² The central surface brightness in the K band for the Bothun and Gregg (1990) sample of S0 is computed from their values in the B band and the B-K color of these galaxies.

shows the location of the PRGs and S0 disks parameters (see also Table 6, in Paper I) in the μ_0^c - $\log r_h$ plane. The same result was found by Reshetnikov et al. 1994 for a sample of PRGs in the B band.

4.5. Bulge-Disk relations

The *Bulge-to-Disk ratio (B/D)* for the host galaxy in PRGs of our sample falls in the range of values typical for disk-dominated S0 galaxies and for spiral galaxies, as shown in Fig. 6 (left panel). The right panel of Fig. 6 shows the correlation between the Bulge-to-Disk ratio (B/D) and the n exponent: as stressed by Möllenhoff & Heidt (2001), for spiral galaxies the B/D decreases with n . The host galaxy of PRGs are characterized by an higher value of the B/D ratio with respect to the spiral galaxies, for the same value of n . This is mostly due to the differences in the disks scalelengths: disks in the PRG host galaxy are much smaller than disks in spiral galaxies (see Sec. 4.4).

5. Study of the light distribution in the polar structure

An important quantity related to the size of the polar ring is the moment of its radial distribution

$$(\Delta R)^2 = \frac{\int_{r_{min}}^{\infty} (r - \bar{R})^2 \mu(r) dr}{\int_{r_{min}}^{\infty} \mu(r) dr} \quad (1)$$

where \bar{R} is the average radius, weighted by the surface brightness distribution, given by

$$\bar{R} = \frac{\int_{r_{min}}^{\infty} r \mu(r) dr}{\int_{r_{min}}^{\infty} \mu(r) dr} \quad (2)$$

and r_{min} is equal to 3 times the effective radius of the central component.

For a pure exponential disk, the $\Delta R / \bar{R}$ ratio tends to unity when r goes to infinity. For a real object, this value is expected to be less than 1, because of its finite extension. This is confirmed by the $\Delta R / \bar{R}$ values derived for a sample of spiral galaxies (de Jong 1996) in the B band: this quantity varies from 45% to 75% and the average value is $\Delta R / \bar{R} \sim 65\%$.

The $\Delta R / \bar{R}$ is a key parameter in the studies about polar ring stability (Sec.1). In order to derive this quantity for every polar ring galaxy in the sample, a folded light profile was computed in the K band, for each object, from the surface brightness profiles extracted along the ring major axis (showed in Fig.4 and Fig.5, Paper I). For the polar ring galaxy ESO 415-G26 the average ring profile was obtained in the B band, where this component is significantly brighter than in the K band (see Sec.7 in Paper I). In Table 2 we list the $\Delta R / \bar{R}$ ratio derived for each polar ring galaxy in the sample: this value is in principle a lower limit, since the polar ring light from regions closer to the host galaxy is not included in the computation. In Fig. 7 these values are compared with the typical $\Delta R / \bar{R}$

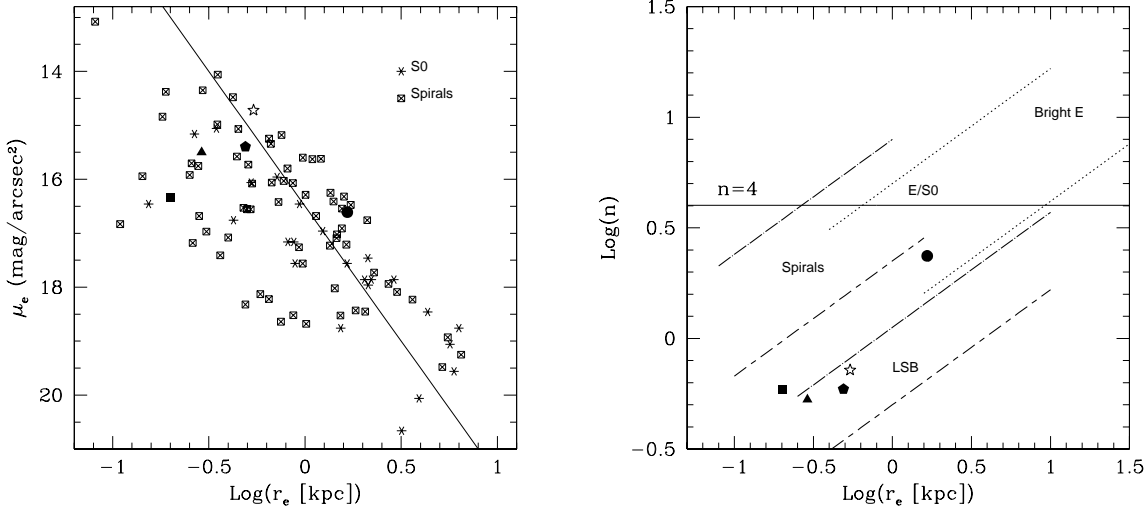


Fig. 4. Left panel - Relation between the bulge effective parameters (see Sec.6 in Paper I) for all PRGs in our sample. Code for symbols is: star for ESO 415-G26, filled square for ARP 230, filled circle for AM 2020-504, filled triangle for ESO 603-G21 and filled pentagon for A0136-0801. They are compared with the typical values for early-type galaxies (Bothun and Gregg, 1990) and for spiral galaxies (Möllenhoff & Heidt 2001; Khosroshahi et al. 2000). The solid line is a line of constant bulge luminosity derived for $\mu_e = 18 \text{ mag/arcsec}^2$, $r_e = 2 \text{ kpc}$ and $n = 4$. Right panel - Relation between the effective radius r_e and the n exponent of the generalized de Vaucouleurs' law (see Sec.6, Paper I), for the bulge component in the PRGs of our sample. They are compared with the typical values for 1) early-type galaxies, Ellipticals and S0s (region limited by dotted lines), by Caon et al. (1993); for 2) LSB galaxies (region limited by dashed lines), by Davies et al. (1988); and for 3) spiral galaxies (region limited by dashed-dotted lines) by Möllenhoff & Heidt (2001) and Khosroshahi et al. (2000). The plotted n exponents values for the early-type galaxies are those derived by Caon et al. (1993) along the minor axis of the system, in order to exclude the contribution from a possible disk component.

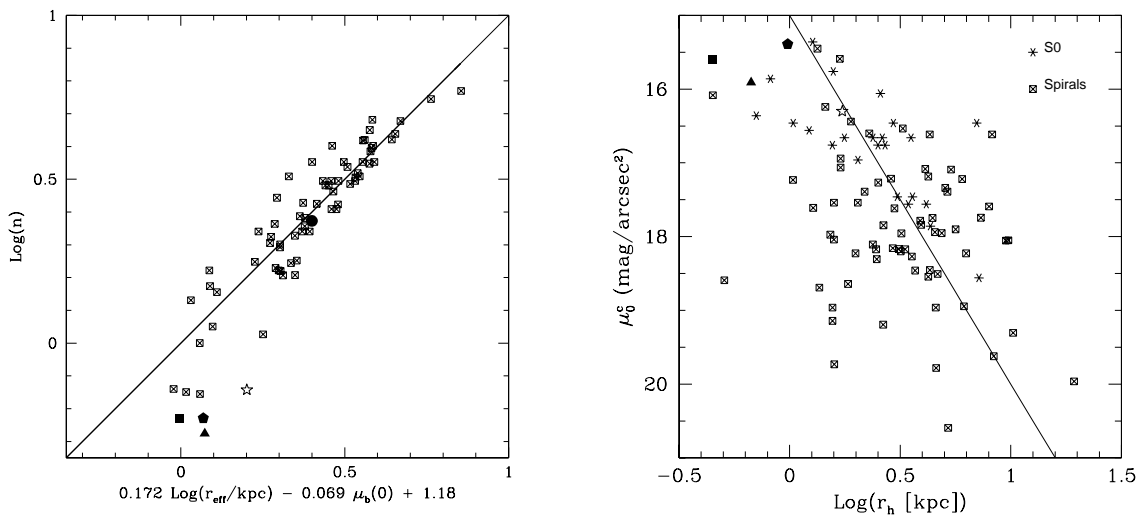


Fig. 5. Left panel - Photometric plane for bulge of spiral galaxies and for PRGs. Right panel - Relation between the central surface brightness, corrected for the inclination, and the scalelength of the disk component in the host galaxy (see Sec.6 in Paper I). Code for symbols is the same adopted in Fig.4. They are compared with the typical values for S0 galaxies by Bothun and Gregg (1990) and for spiral galaxies (Möllenhoff & Heidt 2001; Khosroshahi et al. 2000). The solid line is a line of constant disk luminosity, derived for $\mu_b^c = 18 \text{ mag/arcsec}^2$ and $r_h = 1.6 \text{ kpc}$.

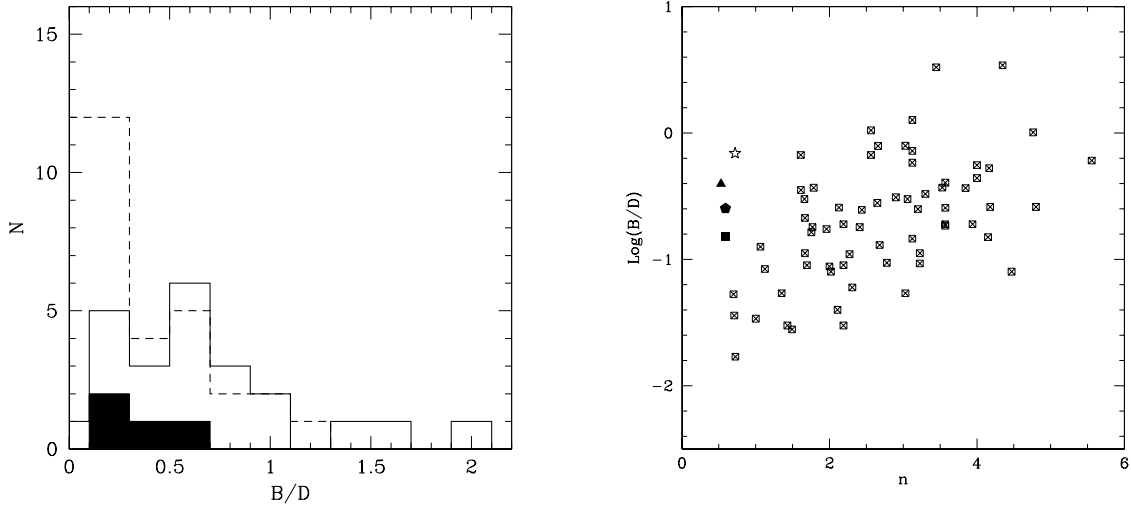


Fig. 6. Left panel - B/D distribution for the PRGs of the sample (filled region), for early-type galaxies, by Bothun and Gregg (1990) (solid line) and for spiral galaxies, by Möllenhoff & Heidt (2001); Khosroshahi et al. (2000). Right panel - Bulge-to-Disk ratio as function of the n exponent, for PRGs and for spiral galaxies. Code for symbols is the same adopted in Fig.4.

Table 2. $\Delta R/\bar{R}$ ratio for polar ring galaxies of the sample.

Object	$\Delta R/\bar{R}$ %
A0136-0801	45
ESO 415-G26	47
ARP 230	35
AM 2020-504	16
ESO 603-G21	39

ratio for annuli in a quasi-equilibrium configuration, derived by Christodoulou et al. (1992) and Katz and Rix (1992) from the stable configuration of PR hydrodynamical simulations. All PRGs in this sample, but AM 2020-504, are outside this range, and have larger $\Delta R/\bar{R}$ ratios. Indeed, a larger number of simulations are needed to test these values for stability, and verify whether those PRGs with a $\Delta R/\bar{R}$ close to 30% may be also considered as quasi-stable structures.

6. Properties of the optical and NIR light distributions in PRGS

Now we summarize which are the main observational properties of the PRGs studied in this work: we firstly discuss about the global characteristics of the central host galaxy and then those relative to the polar structure.

6.1. Is the central component a normal S0 galaxy?

The morphology of the host galaxy in all PRGs of our sample, except for AM 2020-504, resembles that of an S0 galaxy, which is supported by the disk-like structure

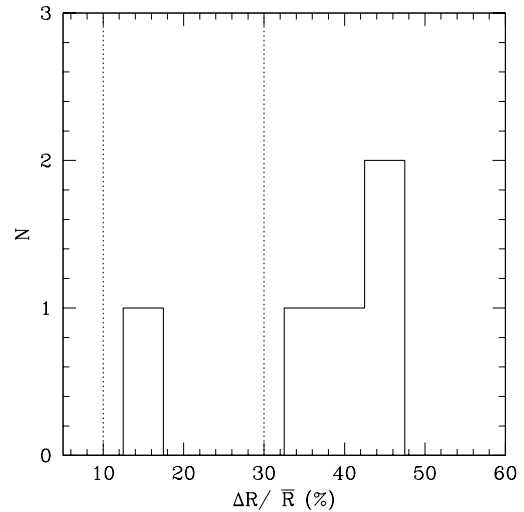


Fig. 7. Distribution of the $\Delta R/\bar{R}$ ratio derived for each polar ring galaxy in the sample. The dotted lines limit the range of $\Delta R/\bar{R}$ ratio for annuli in a quasi-equilibrium configuration, formed in the accretion/merging scenario in the simulations reported by Christodoulou et al. (1992) and Katz & Rix 1992.

present along their major axis. However, a detailed study of the light and color distributions have shown that this component differs from a “standard” S0 galaxy. The mean colors of the stellar component outside the nucleus are, on average, bluer than the typical values for elliptical and S0 galaxies; this is found in nearly all objects. Furthermore,

in all systems a color gradient toward bluer colors is observed from the nucleus to the outer regions. We found that most of the light comes from stars whose mean age varies between 1 and 3 Gyrs, which is significantly younger than the typical age for early-type galaxies. The 2D model of the host galaxy light distribution, performed in the Kn band, has shown that this component is reproduced by a nearly exponential bulge and an outer exponential disk. The analysis of their structural parameters suggests that the host galaxy in PRGs is characterized by a more “compact” bulge with respect to that in S0 galaxies, and by a brighter and smaller disk than that of a typical S0’s disk. In particular, the PRGs bulge scale parameters, except for AM 2020-504, are similar to those of late-type galaxies rather than to those of early-type systems. The resulting B/D ratio is in the range expected for disk-dominated S0 galaxies and for spiral galaxies. All PRG bulges, except for AM 2020-504, tends to be outside from the photometric plane which characterizes elliptical galaxies and the bulge of spiral galaxies. This evidence suggests that the host galaxy in all PRGs, except for AM 2020-504, may have had a different formation history respect to Ellipticals and spiral bulges.

6.2. Is the polar ring similar to a spiral disk?

In all PRGs of our sample the colors of the polar structure fall in the same regions where late-type systems, dwarf and spiral galaxies, are also found; they are, on average, bluer than the central host galaxy, implying a younger age for this component. In all PRGs studied in this work, the light of the polar ring comes predominantly from stars not older than 1 Gyr, which is comparable with younger spiral galaxies. An interesting result was derived by studying the light distribution of the polar structure in all objects of the sample: the ratio between its radial extension (ΔR) and its mean radius (\bar{R}) varies in the range from 35% to 50%, with the exception of AM 2020-504, whose polar ring is characterized by a significantly smaller $\Delta R/\bar{R}$ (about 10%). The typical value of $\Delta R/\bar{R}$ for spiral galaxies varies from 45% to 75%.

Previous studies on PRGs, including also the objects in our sample, have shown that they are characterized by a very large amount of HI gas, which is always associated to the polar structure (van Gorkom et al. 1987; Arnaboldi et al. 1997; van Driel et al. 2000). The total amount of HI is especially high, when compared with the gas content of normal S0 galaxies, which often have no detectable HI. The HI mass in the polar ring galaxies studied in this work is larger than $10^9 M_{\odot}$ (see Sec. 7 in Paper I for more details). For a reasonable mass-to-light ratio ($M/L \sim 2$ in the NIR, from Matthews et al. 1998) we found that the total baryonic mass (gas plus stars) in the polar structure for all PRGs, but AM 2020-504, is comparable with, or even higher than, the total luminous mass in the host galaxy (see Table 3).

7. Conclusions

In this work we have presented the analysis of the detailed photometric study for a sample of PRGs, selected from the Polar Ring Catalogue (PRC, Whitmore et al. 1990), based on new NIR observations presented in Iodice et al. 2002b (Paper I). We now wish to compare the properties predicted for PRGs in different formation scenarios, presented in Sec.1 (see also Iodice et al. 2002a), against the global properties observed for the polar ring systems studied in this work.

For all PRGs of our sample, except for AM 2020-504, the published simulations of the accretion/stripping scenario are so far not able to predict

1. the main characteristics in the light and color distribution of the host galaxy, which make this component different from a standard S0 system;
2. the large values for the $\Delta R/\bar{R}$ ratio, which is related to the ring extension;
3. the large baryonic mass (stellar + gas), shown in Table 3, in the polar ring.

The observed properties for AM 2020-504 (see Sec.7 in Paper I) suggest that this polar ring may be the single case in our sample which may be formed through an accretion or gas-stripping involving an elliptical galaxy.

All the observed properties of the host galaxy and polar structure can be more easily explained by the dissipative merger scenario proposed by Bekki (1998). In this scenario both the central S0-like system and ring component in a polar ring galaxy are simultaneously formed through a dissipative merger between two disk galaxies. The required constraints on the specific orbital configurations and gaseous dissipation in galaxy merging naturally explain the prevalence of S0-like systems among polar ring galaxies (e.g., Whitmore 1991) and the appreciably larger amount of interstellar gas in PRGs (van Gorkom et al. 1987, Arnaboldi et al. 1997, van Driel et al. 2000). This scenario does predict peculiar characteristics for the host galaxy: the progenitor galaxy (the intruder) experiences both a heating of the disk (it puffs up) and energy dissipation. The energy dissipation leads to an higher increase of the mass density in the center, with respect to the unperturbed disk, which may develop a central small and nearly exponential bulge: this is very similar to what we have detected in nearly all PRGs of our sample. The evolutionary timescales of the merging process, which is about 10^9 yr, is also consistent with the young age, predicted for PRGs in this work, both for the host galaxy (1 to 3 Gyr) and polar structure (~ 1 Gyr). Furthermore, the different morphologies observed for polar rings, such as narrow rings (e.g. ESO 415-G26, or in ARP 230) and wide disk-like structures with no central hole (e.g. NGC 4650A, see Iodice et al. 2002a and Gallagher et al. 2002), are related to the orbital parameters of galaxy merging and the initial mass ratio of the two interacting galaxies.

An important constraint to the Bekki scenario is the small value of the relative velocities ($V \sim 33$ km s $^{-1}$) that

Table 3. Mass of the stellar component in the host galaxy (second column) and the total baryonic mass in the polar structure (third column), which includes the mass of the stellar component and the mass of the gas in the form of neutral (HI) and molecular hydrogen (HII). See Sec.7, Paper I for additional references.

Object	M_{star} (HG) $10^9 M_\odot$	$M_{gas} + M_{star}$ (PR) $10^9 M_\odot$
ESO 415-G26	9	10
ARP 230	2	5
AM 2020-504	6	5
ESO 603-G21	2	10

the two merging galaxies need to have to form PRGs: such velocities are more likely to occur in high redshift universe rather than nearby, where bound group of galaxies are virialized and therefore their relative velocities are larger. Reshetnikov (1997) have found an increasing rate of detection for PRGs toward higher redshift: among all galaxy types, in the Hubble Deep Field (Williams et al. 1995) candidate polar ring galaxies are $\sim 0.7\%$, while in the local universe this is $\sim 0.05\%$ (Whitmore et al. 1990). Although uncertainties in the numerical treatment of gas dynamics and star formation still remain in the Bekki's approach, dissipative galaxy merging, with specific initial conditions, seems now a promising scenario to explain the formation of Polar Ring Galaxies and their observational properties.

Acknowledgements. The authors wish like to thank the referee, V. Reshetnikov, whose comments and suggestions helped to improve this work. E.I and M.A. wish to thank Prof. Capaccioli and the staff of the Observatory of Capodimonte for the help and support during the realization of this work. E.I. and M.A. would like to thank G. De Lucia for the help in the use of GISSEL, the stellar population synthesis model.

References

Aaronson, M., Cohen, J., Mould, J. and Malkan, M. 1978, AJ, 223, 824

Arnaboldi, M., Freeman, K. C., Sackett, P. D., Sparke, L. S. and Capaccioli, M., 1995, PASP, 43, 1377

Arnaboldi, M., Oosterloo, T., Combes, F., Freeman, K. C. and Koribalski, B., 1997, AJ, 113, 585

Bekki, K. 1998, ApJ, 499, 635

Bekki, K., 1997, ApJ, 490, L37

Bergvall, N., Ronnback, J., Masegosa, J. and Ostlin, G. 1999, A&A, 341, 697

Bothun, G. D. and Gregg, M. D. 1990, ApJ, 350, 73

Bothun, G. D., Romanishin, W., Strom, S. E. and Strom, K. M. 1984, AJ, 89, 1300

Bothun, G. D. 1982, ApJS, 50, 39

Bruzual, G. and Charlot, S. 1993, ApJ, 405, 538

Caon, N., Capaccioli, M. and Capaccioli, M. 1993, MNRAS, 265, 1013

Capaccioli, M., Caon, N. and D'Onofrio, M., 1992, MNRAS, 259, 323

Charlot, S., Worthey, G. and Bressan, A. 1996, ApJ, 457, 625

Christodoulou, D. M., Katz, N., Rix, H. W. and Habe, A. 1992, ApJ, 395, 113

Davies, J. I., Phillipps, S., Cawson, M. G. M., Disney, M. J. and Kibblewhite, E. J., 1988, MNRAS, 232, 239

de Jong, R. S. 1996, A&AS, 118, 557

de Jong, R. S. and van der Kruit, P. C. 1994, A&AS, 106, 451

Driver, S.P., Windhorst R.A., Ostrander E.J., Keel W.C., Griffiths R.E. and Ratnatunga K.U., 1995, ApJ, 449, L23

Frogel, J. 1985, ApJ, 298, 528

Frogel, J., Cohen, J. and Persson, E. 1983, AJ, 275, 773

Gallagher, J.S., Sparke, L.S., Matthews, L.D., Frattare, L.M., English, J., Kinney, A.L., Iodice, E., Arnaboldi, M. 2002, ApJ, 568, 199

Giovanardi, C. and Hunt, L. K. 1996, AJ, 111, 1086

Glass, I. S. and Moorwood, A.F.M., 1985, MNRAS, 214, 429

Gordon, K. D., Calzetti, D. and Witt, A. N. 1997, ApJ, 487, 625

Hibbard, J. E. and Mihos, J. C., 1995, AJ, 110, 140

Iodice, E., Arnaboldi M., De Lucia, G., Gallagher, J.S., Sparke, L.S. and Freeman, K.C. 2002, AJ, 123, 195

Iodice, E., Arnaboldi M., Sparke, L.S., Gallagher, J.S. and Freeman, K.C. 2002, A&A, Paper I

Katz, N. and Rix, H. 1992, ApJ, 389, L55

Khosroshahi, H.G., Wadadekar, Y. and Kembhavi, A., and Mobasher, B., 2000, ApJ, 531, L103

Khosroshahi, H.G., Wadadekar, Y. and Kembhavi, A., 2000, ApJ, 533, 162

Kennicutt, R. C., Jr., 1983, ApJ, 272, 54

Li, J.G. and Seaquist, E. R., 1994, AJ, 107, 1953

Matthwes, L.D., van Driel, W. and Gallagher, J.S. 1998, AJ, 116, 2196

Möllenhoff, C. and Heidt, J. 2000, A&A, 368, 16

Persson, S. E., Frogel, J. A. and Aaronson, M. 1979, ApJS, 39, 61

Reshetnikov, V. and Sotnikova, N. 1997, A&A, 325, 933

Reshetnikov, V.P. 1997, A&A, 321, 749

Reshetnikov, V. P., Hagen-Thorn, V. A. and Yakovleva, V. A., 1996, A&A, 314, 729

Reshetnikov, V. P., Hagen-Thorn, V. A. and Yakovleva, V. A., 1994, A&A, 290, 693

Sackett, P., 1991, in Warped Disks and Inclined Rings around Galaxies, ed. S. Casertano, P. Sackett and F. Briggs (New York: Cambridge Univ. Press), p.73

Salpeter, E. E. 1955, ApJ, 121, 161

Schweizer, F., Whitmore, B. C. and Rubin, V. C., 1983, AJ, 88, 909

Shane, W.W., 1980, A&A, 82, 314

Sparke, L.S., 1991 in Warped Disks and Inclined Rings around Galaxies, ed. S. Casertano, P. Sackett and F. Briggs (New York: Cambridge Univ. Press), p.85

Thuan, T. X. 1985, ApJ, 299, 881

Toomre, A., 1977, ARA&A, 15, 437

van Driel, W., Arnaboldi, M., Combes, F. and Sparke, L. S., 2000, A&AS, 141, 385

van Gorkom, J. H., Schechter, P.L. and Kristian, J., 1987, ApJ, 314, 457

Whitmore, B. C. 1991, in Warped Disks and Inclined Rings around Galaxies, ed. S. Casertano, P. Sackett and F. Briggs (New York: Cambridge Univ. Press), 60

Whitmore, B. C., Lucas, R. A., McElroy, D. B., Steiman-Cameron, T. Y., Sackett, P. D. and Olling, R. P. 1990, AJ, 100, 1489

Williams, R., Dickinson, M., Giavalisco, M., Gilliland, R., Ferguson, H., Fruchter, A., McElroy, D., Lucas, R., Petro, L., Postman, M., American Astronomical Society Meeting, 187